TITLE: Abiotic Dechlorination in the Presence of Ferrous Minerals

AUTHORS: Charles E. Schaefer[1,*], Paul Ho[2], Erin Berns[3], Charles Werth[3]

AFFILIATIONS: [1] CDM Smith, 110 Fieldcrest Avenue, #8, 6th Floor, Edison, NJ 08837

[2] CDM Smith, 14432 SE Eastgate Way # 100, Bellevue, WA 98007

[3] University of Texas at Austin, Civil, Architectural, and Environmental Engineering, 301 E. Dean Keeton St., Stop C1786, Austin, TX 78712

[*]**CORRESPONDING AUTHOR**: Mailing address: CDM Smith, 110 Fieldcrest Avenue, #8, 6th Floor, Edison, NJ 088837. (732)-590-4633. E-mail: schaeferce@cdmsmith.com

Submitted to the *Journal of Contaminant Hydrology*

Key Words: TCE, abiotic, ferrous minerals, dechlorination

Abstract

Laboratory batch experiments were performed to assess the reduction of trichloroethene (TCE) and oxygen via natural ferrous minerals. TCE reduction under anoxic conditions was measured via the generation of reduced gases, while oxygen reduction via the generation of hydroxyl radicals was measured as a surrogate for potential TCE oxidation. Results showed that TCE reduction under anoxic conditions was observed for ankerite, siderite, and illite, but not for biotite; acetylene was the primary identified dechlorination product. With the exception of biotite, first-order dechlorination rate constants increased with increasing ferrous content of the mineral, with rate constants ranging from 3.1×10^{-8} to $4.8\ 10^{-7}$ L g^{-1} d^{-1}. Measured reduction potentials (mV vs SHE) ranged from -104 for illite to +84 for biotite. When normalizing measured first-order dechlorination rate constants to the estimated ferrous iron mineral specific surface area (where surface area was based on nitrogen adsorption analysis of the minerals). TCE dechlorination rate constants increased with increasing reduction potentials. Under oxic conditions, hydroxyl radicals were generated with each of the four minerals. However, mineral activity showed no readily apparent correlation to ferrous content or mineral surface area. In terms of TCE and oxygen reduced per mole of ferrous iron initially present in each mineral, illite was the most reactive of the four minerals. Together, these results suggest that several ferrous minerals may contribute to abiotic dechlorination in the natural environment, and (at least for TCE reduction under anoxic conditions) measurement of ferrous mineral content and reduction potential may serve as useful tools for estimating TCE first-order abiotic dechlorination rate constants.

1.0 Introduction

The diffusive uptake or release of chlorinated solvents such at trichloroethene (TCE) and tetrachloroethene (PCE) from low permeability rock or clay matrices can have a substantial impact on contaminant migration and longevity within impacted aquifers, as previous studies have shown that these matrices can serve as a long-term source of these compounds (Damgaard et al., 2013; Goode et al., 2014). Slow abiotic dechlorination reactions in such matrices can impact diffusive uptake and release (West and Kueper, 2010; Schaefer et al., 2013; Schaefer et al., 2016; Schaefer et al. 2017; Yu et al., 2018), and therefore limit contaminant longevity. The mechanisms controlling abiotic dechlorination reactions and methods to predict reactivity remain on-going issues of debate, and further insights are needed to effectively manage impacted sites.

There is substantial evidence that ferrous minerals play a prominent role in promoting abiotic reductive dechlorination of PCE and TCE (Butler and Hayes, 1999; Liang et al., 2009; He et al., 2010; He et al., 2015; Schaefer et al., 2017). The majority of these studies were performed under anoxic conditions with single minerals, and suggest that ferrous minerals such as pyrite, iron sulfides, magnetite, and green rusts can dechlorinate PCE and TCE to yield short-chained hydrocarbons (e.g., acetylene, ethene, ethane, propane) as final products (Lee and Batchelor, 2003; Schaefer et al., 2013; He et al., 2015). However, there is also evidence that in studies performed with these and other iron minerals, small amounts of unidentified reactive mineral intermediates (RMIs) are promoting chlorinated ethene reduction. (Culpepper et al., 2018; Entwistle et al., 2019).

The iron minerals controlling reactivity are more difficult to determine in natural systems. Several researchers have shown that iron-containing rock and clay matrices

promote PCE and TCE dechlorination under anoxic and abiotic conditions (Schaefer et al., 2017; Yu et al., 2018; Schaefer et al., 2018), and that this reactivity can persist in situ after decades of exposure to the contaminants (Ferry et al., 2004; Schaefer et al., 2015; Schaefer et al., 2018b). Furthermore, the abiotic dechlorination rate constants observed in these natural matrices have been shown to be environmentally relevant (Schaefer et al., 2013, 2018; 2018b; Berns et al., 2019). In one study, the observed first-order dechlorination rate constants for natural clayey soils was directly correlated to the ferrous mineral content of the solids determined via HCl extraction (Schaefer et al., 2018). However, XRD results indicated that these matrices contained several ferrous iron minerals, and no relationship to their relative proportions was apparent. Therefore, it remains unclear what specific ferrous minerals might be responsible for the observed abiotic dechlorination in natural systems, or if the mechanisms responsible for dechlorination reactions in altered natural minerals differ from those in artificially reduced minerals.

In addition to reducing chlorinated ethenes, ferrous iron minerals have also been shown to reduce oxygen to form hydroxyl radicals and hydrogen peroxide under oxic conditions (Pham et al., 2008; Kong et al., 2015; Tong et al., 2016; Morrison et al., 2016). In natural clays containing ferrous minerals, this hydroxyl radical generation process was observed, with subsequent oxidative dechlorination of TCE at rates much greater than the reductive TCE dechlorination observed under anoxic conditions (Liu et al., 2017; Schaefer et al., 2018). The extent of hydroxyl radical yield per mass of ferrous iron depends on the type of ferrous mineral, suggesting a complex mechanism related to the mineral structure likely is involved (Tong et al., 2016; Zhu et al., 2019). While the extent

to which these abiotic oxic dechlorination processes are relevant to the diffusion of chlorinated ethenes into clay or rock matrices is unclear, field studies suggest that systems undergoing natural biogeochemical cycling might be conducive to such processes (Page et al., 2013; Tong et al., 2016; Yuan et al., 2017).

Besides extracted ferrous iron discussed above, the soil reduction potential, determined electrochemically or with chemical reactivity probes, is also being explored as a surrogate for reductive dechlorination rate constants in natural soils and minerals under anoxic conditions (Fan et al., 2016; Kocur et al., 2020). However, to our knowledge, this work has yet to be extended to PCE or TCE, which are reduced via ferrous minerals much more slowly than the carbon tetrachloride, 4-chloronitrobenzene, and 2-chloroacetophenone used by Kocur et al. (2020) and Fan et al. (2016). In addition, it is currently unclear the extent to which reduction potential measurements provide insight into hydroxyl radical formation observed for ferrous minerals under oxic conditions. The ability to relate reduction potential via chemical reactivity probes to hydroxyl radical generation could serve as a surrogate relating to abiotic TCE oxidation, as the extent of hydroxyl radical generation has been shown to correspond to the subsequent oxidative dechlorination of TCE in batch systems (Pham et al., 2008; Schaefer et al., 2018).

While previous studies have focused on TCE dechlorination via ferrous minerals, comparison of reductive TCE dechlorination kinetics among various minerals coupled with the ability to predict such dechlorination using ferrous iron content and reduction potentials, has not to our knowledge been performed. The purpose of this study was to interrogate the potential for abiotic dechlorination using individual minerals identified in

131 natural clay sediments (illite, biotite, ankerite, and siderite) that were suspected to be
132 responsible for reducing TCE (Schaefer et al., 2018), and to compare the various minerals
133 with respect to TCE dechlorination kinetics. Both TCE reduction under anoxic conditions
134 and hydroxyl radical generation under oxic conditions were examined. Specifically,
135 mineral reduction of both TCE and oxygen (as evidenced by hydroxyl radical generation)
136 were compared, thereby providing insight into the reduction mechanisms and potential
137 behavior in systems where iron redox cycling may occur. In addition, assessment of
138 ferrous iron content and reduction potential as tools to estimate TCE reduction under
139 anoxic conditions and hydroxyl radical generation under oxic conditions were examined,
140 thereby providing a novel assessment of these techniques.
141

142 **2.0 Experimental**

143 *2.1 Materials*

144 TCE (>99.5% purity), and reduced gas standards (15 ppm methane, ethane, ethene,
145 acetylene, propane, propylene, methyl acetylene, butane in a nitrogen balance) were
146 purchased from Sigma Aldrich (St. Louis, MO). An electrolyte solution consisting of 5
147 mM $CaCl_2$ was used in all experiments. Four natural minerals samples were used for this
148 study. Siderite (purchased from SIDCO Minerals Inc., Texarakana, TX), illite (purchased
149 from greenclays.com, Las Vegas, NV), biotite (acquired black crystal from unknown
150 location in Ontario, CA; additional samples available at https://www.ebay.com/itm/13-
151 Rare-Shining-Biotite-Crystal-Black-Mica-Ontario-Canada-Mica110-/303174730742),
152 and ankerite (mineral crystal acquired from unknown location in Eisenerz, Steiermark,

153 Austria) were used for the abiotic reactivity experiments. Properties of the minerals are
154 provided in Table 1.
155
156 *2.2 Batch Dechlorination Testing*
157 Using previously developed methods (Schaefer et al., 2017; Schaefer et al., 2018),
158 batch experiments were performed under anoxic conditions to evaluate the abiotic
159 reductive dechlorination of TCE. All anoxic experiments were prepared in an anaerobic
160 chamber. For each batch system, 6 g of a specific mineral was placed in 40 mL amber
161 glass vials. Bottles were then amended with 35 mLs of 5 mM $CaCl_2$ that had been
162 sparged with nitrogen. An additional set of bottles were prepared similarly, but amended
163 with TCE for a concentration of approximately 3.2 mM. Use of elevated TCE
164 concentrations facilitated the detection of transformation products. For siderite and illite,
165 additional experiments were performed at a TCE concentration of approximately 0.15
166 mM. Comparison of samples amended with TCE to those without TCE served to verify
167 that generation of suspected dechlorination products were from TCE, rather than
168 generation from anything associated with the acquired minerals.
169 The vials were capped with Mininert valves (with epoxy seals on the threads) to allow
170 for repeated sampling of the vial headspace for hydrocarbon transformation products. All
171 anoxic experimental conditions were prepared in triplicate (i.e., vials were prepared in
172 triplicate for each condition). Controls, containing 5 mM $CaCl_2$ solution with TCE but no
173 minerals, also were prepared in triplicate.
174 All sampling of the anoxic vials was performed outside of the anaerobic chamber
175 under a stream of nitrogen to limit potential introduction of oxygen into the vials.

176 Monitoring was typically performed up to approximately 40 days. At the end of the
177 experiment, select vials were sampled to determine the pH in the supernatant water. An
178 additional set of experiments was performed using illite and siderite amended with 1.8
179 mM of ferrous iron (from $FeCl_2$-H_2O); these experiments were performed in duplicate.
180 Oxic experiments were also prepared similarly to those previously described
181 (Schaefer et al., 2018), and as described above for the anoxic experiments. The purpose
182 of the oxic experiments was to measure hydroxyl radical generation. Thus, here we use
183 hydroxyl radical measurements as a surrogate for comparing the relative oxidative abiotic
184 dechlorination potential among the four minerals.
185 For oxic experiments, the focus was to measure the generation of hydroxyl radicals,
186 which have shown to subsequently and oxidatively dechlorinate TCE (Pham et al., 2008;
187 Liu et al., 2017; Schaefer et al., 2018). Thus, the extent of hydroxyl radical generation
188 among the four ferrous minerals served as a surrogate for evaluating their relative
189 potential effectiveness to facilitate oxidative transformation of TCE. Hydroxyl radical
190 generation was measured using the aminophenyl fluorescein (APF) method (Cohn et al.,
191 2008; Cohn et al., 2009), which is based upon hydroxyl radical transformation of the APF
192 into fluorescein. For each mineral, 1.7 g were placed in the 40 mL amber glass vials with
193 10 mL of 0.1 M phosphate buffer (pH=7.4). Vials also were amended with APF to attain
194 a 25 µM concentration. With the bottle headspace flushed with air at time zero and daily
195 thereafter, periodic aqueous samples were collected during the 6-day duration of the
196 experiments. Bottles were placed on a shaker (50 rpm) during incubation.
197 Periodic sampling was performed by removing a 400 µL aliquot that was transferred
198 into a 15mL conical centrifuge tube and centrifuged at 10,000 g for 5 minutes. The

supernatant was subsequently analyzed using a Promega Quantus Fluorometer, where a blue fluorescent channel with an excitation filter at 495nm and emission filter at 510-580nm was used to quantify fluorescein. All samples, including a control containing no minerals, were prepared in duplicate.

2.3 Analytical Methods, Calculation of Dechlorination Rate Constants, and Soil Characterization

TCE, *cis*-1,2-dichloroethene (DCE), vinyl chloride (VC), and reduced gas (methane, ethane, ethene, propane, acetylene, butane, methyl acetylene, and propylene) concentrations were determined via headspace analysis using a Shimadzu 2010+ gas chromatograph equipped with a Flame Ionization Detector (FID) and an RT-QS-BOND fused silica PLOT column. Aqueous concentrations were determined by applying Henry's Law.

TCE reductive dechlorination in the anoxic systems are described by the following first-order expression (Schaefer et al., 2017; Schaefer et al., 2018):

$$\frac{\partial C}{\partial t} = \frac{k_{an}}{\frac{\varepsilon_v H + \varepsilon_w}{\varepsilon_w}} C \qquad \text{Eq. 1}$$

$$k_{an} = k'_{an} \frac{\rho K}{\varepsilon_w} \qquad \text{Eq. 2}$$

where C is the TCE aqueous concentration (mM), t is time (days), k_{an} is the bulk first order rate constant (d^{-1}), k'_{an} is the intrinsic pseudo first order rate constant (d^{-1}), ρ is the bulk density (0.2 kg L^{-1}), K is the linear TCE adsorption coefficient to both reactive and unreactive sites (L kg^{-1}), ε_v and ε_w are the dimensionless gas and water porosities in the vial (0.20 and 0.74, respectively), and H is the TCE dimensionless Henry's Law constant (Sander, 1999). Since the adsorption of TCE to the reactive ferrous minerals cannot be

222 determined, the reaction rate constant is assessed in terms of k_{an} rather than k'_{an}. For Eq.
223 1, generation of acetylene + ethene is used to determine the change in TCE concentration.
224 This approach has been employed previously (Schaefer et al., 2017).
225 A small (approximately 10%) TCE leakage loss was observed in the controls at the
226 final (40 day) sampling point due to volatilization losses from the vials. Reduced gas
227 transformation products were corrected for this loss using a Henry's Law based
228 partitioning factor to account for losses of transformation products as follows (Schaefer et
229 al., 2017):
230 $$\alpha_i = \frac{\varepsilon_v + \frac{\varepsilon_w}{H_{TCE}}}{\varepsilon_v + \frac{\varepsilon_w}{H_i}} \quad \text{Eq. 3}$$
231 where α_i is the scaling factor by which TCE dechlorination product i is multiplied to
232 correct for leakage losses. H_i is the dimensionless Henry's Law constant for TCE and
233 dechlorination product i (Sander, 1999).
234 Ferrous mineral content was determined using a 2.5% HCl extraction and the 1,10-
235 phenanthroline method (Standard Method 3500-Fe B.4.c, Rice et al., 2012); this
236 methodology has been used in previous studies that showed a correlation between ferrous
237 mineral content and reductive TCE dechlorination rate constants (Schaefer et al., 2017;
238 Schaefer et al., 2018). An additional more aggressive ferrous iron extraction was also
239 performed using 12.5% HCl and with heated (95 C) water bath. Both of these ferrous
240 mineral extractions were performed by McCampbell Analytical, Inc. (Pittsburg, CA).
241 Reduction potentials were measured after equilibrating minerals in anoxic
242 bicarbonate buffer by shaking in an anaerobic chamber overnight. Three mediator
243 compounds (indigo tetrasulfonate, indigo disulfonate, and athraquinone disulfonate) were
244 used to determine the potentials in the mineral slurries; this approach has been shown to

be appropriate for predicting abiotic dechlorination using soil and mineral samples (Fan et al., 2016; Kocur et al., 2020). Potentials were measured anaerobically with a Ag/AgCl (3 M KCl) Mettler Toledo Redox Micro ORP Electrode, and converted to SHE; this approach has been shown, using field-collected soil samples, . The electrode was rinsed in 0.1 N HCl for 30 minutes between each sample. All reduction potential measurements were performed in at least duplicate.

3.0 Results and Discussion

3.1 Anoxic Experiments

The molar fraction of TCE transformed to reduced gas products for each mineral over the 40 day experiment is shown in Figure 1. Acetylene was the primary transformation product observed, accounting for > 90% of the observed TCE transformation. The remaining TCE removal was accounted for as ethene generation. No chlorinated ethene or reduced gas transformation products were observed in the controls (no minerals present), and TCE concentrations in the controls were statistically identical to those in the mineral-amended bottles indicating that TCE sorption to the minerals was below that which could be measured in this study (< 1.8 mmol kg^{-1}). Trace levels of reduced gas transformation products were observed in the experiments with minerals without TCE present, but these trace levels of reduced gases were less than 1% of those observed in the TCE-amended samples (with the exception of biotite, where no measurable generation of transformation products relative to the non-TCE amended samples was observed).

Acetylene is not a known biotic TCE transformation product, and therefore the generation of acetylene as the primary dechlorination product provides strong evidence

268 that the TCE dechlorination occurred via an abiotic reductive mechanism. TCE abiotic
269 reductive dechlorination typically occurs via a reductive beta-elimination pathway, with
270 the formation of acetylene, and with possible further reduction to ethene (Roberts et al.,
271 1996; Arnold and Roberts, 2000; Schaefer et al., 2018). Ethene has been shown to be an
272 abiotic TCE dechlorination product in ferrous mineral studies (Lee and Batchelor, 2003;
273 Entwistle et al., 2019), but can also be attributed to the biotic transformation of TCE
274 (Cápiro et al., 2015; Schaefer et al., 2009). No other biotic TCE dechlorination products
275 (i.e., DCE, VC) were detected, suggesting that the ethene generation likely was due to
276 abiotic mechanisms. Previous abiotic TCE dechlorination experiments using natural
277 clayey soils that (based on soil mineral analysis) contained minerals similar to those
278 studied herein also primarily yielded acetylene and/or ethene as abiotic reductive
279 transformation products under anoxic conditions (Schaefer et al. 2018). Results presented
280 in Figure 1 show that siderite, illite, and ankerite each facilitates the abiotic reductive
281 dechlorination of TCE, suggesting that the presence of these minerals in previously
282 examined natural clayey soils likely played a role in TCE dechlorination.
283 Table 2 shows regressed first-order TCE reductive dechlorination rate constants on
284 both a mass and estimated mineral surface area basis. Regression results indicate that
285 dechlorination was reasonably described (R^2 values typically greater than 0.9) by a first-
286 order expression, consistent with previous abiotic dechlorination studies in the presence
287 of ferrous minerals (Butler and Hayes, 1999; Schaefer et al., 2013). However, it is noted
288 that because the fraction of TCE consumed was low which resulted in essentially a
289 constant concentration of TCE during the experiment, the data provided in Figure 1 are
290 unable to discern between a zero- and first-order rate model with respect to TCE

291 concentration. In addition, the initial (t=1 day) timepoint for siderite was not used in the
292 first-order regressions, as a relatively rapid rate of dechlorination occurred between t=1
293 and t=7 days. This transient rate of high dechlorination activity may have been due to
294 consumption and depletion of a highly reactive iron species.

295 First-order TCE reductive rate constants obtained herein, along with those obtained in
296 a previous study using similar methodologies with natural clayey soils (Schaefer et al.,
297 2018) are plotted as a function of the ferrous iron content (Figure 2). With the exception
298 of the visibly outlying biotite mineral, the TCE dechlorination rate constant generally
299 increases with increasing ferrous content, which is consistent with previous studies
300 (Schaefer et al., 2013; Schaefer et al., 2018). Together, these results suggest that ferrous
301 minerals facilitate the observed reductive dechlorination reactions under anoxic
302 conditions. It is noted that the first order rate constants measured herein (with the
303 exception of that measured for biotite) are sufficiently large such that they would likely
304 be of environmental relevance for mitigating TCE persistence in clay or rock matrices
305 (Schaefer et al., 2018; 2018b, Berns et al., 2019).

306 The relationship between the dechlorination rate constant and ferrous mineral content
307 in Figure 2 is surprising, as the solids used varied in the degree of heterogeneity
308 (predominantly single minerals versus natural solids containing multiple mineral species),
309 surface area, and particle size. Multiple factors may contribute to this relationship. One
310 contributing factor likely is that the reaction rate constants are very slow. This can be
311 assessed by comparing the reaction to diffusion velocities in terms of the dimensionless
312 Da number (Cussler, 1994):

313 $$Da = \frac{k_{an} L^2}{D}$$ Eq. 4

where L is the diffusion length, and D is the effective aqueous diffusion coefficient that accounts for the tortuosity within the clay. For reactions that are very slow relative to the diffusional mass transfer, Da << 1. Assuming an effective diffusion coefficient of 2 x 10^{-5} cm^2 d^{-1} (Werth et al., 1997) and a diffusion length of 0.001 cm (based on the mineral particle sizes), a reasonable estimate of the diffusion velocity (D L^{-2}) is 20 d^{-1}. This value is more than 6 orders of magnitude greater than the first order rate constants shown in Table 2, ensuring that Da << 1. This explains why the variation in particles sizes and surface areas among the solids do not appear to impact results.

Another potential contributing factor is that the acid extraction used to determine the ferrous content for the minerals and soils may be sensitive to the factors that control the reactivity of the ferrous minerals with respect to TCE reductive dechlorination, thereby facilitating the observed trend observed in Figure 2. The 2.5% HCl acid extraction (Table 1) likely did not extract all of the ferrous iron present in the solids, but rather the most extractable iron, which is likely a function of accessibility, surface area, and coordination within the mineral structure. The relatively low measured ferrous content for siderite (36 g kg^{-1}) is consistent with this interpretation, because the ferrous content based only on stoichiometric mineral composition should be more than 10-times greater. The latter was confirmed by the heated acid extraction data for siderite, which matches closely with the theoretical ferrous content of 482 g kg^{-1} based on stoichiometry ($FeCO_3$) (Table 1).

The results presented herein and previously (Schaefer et al., 2013; Schaefer et al., 2017; Schaefer et al., 2018) suggest that abiotic reductive dechlorination under anoxic conditions is positively correlated to the ferrous mineral content. These results are in apparent contrast to recent mechanistic studies (Culpepper et al., 2018; Entwistle et al.,

2019) that show ferrous minerals alone do not dechlorinate TCE, nor does the ferrous mineral content correlate to observed dechlorination rates; rather, Culpepper et al. and Entwistle et al. suggest RMIs are responsible for the observed dechlorination. One possible explanation for this apparent discrepancy is that the reductive dechlorination reactivity observed herein is in fact due to these RMIs that have accumulated near the mineral surfaces, and the measured ferrous mineral contents (Table 1) reflect (in part) the quantity of these reactive particles. A second consideration is that the dechlorination rate constants for unaltered natural minerals and soils (such as those employed herein) occurs via a different – and much slower – mechanism than that observed for RMIs (Entwistle et al., 2019). If the mineral (6 g L^{-1}) and TCE (0.07 mM) dosage used in the batch experiments performed by Entwistle et al. (2019) were used for the minerals examined herein, no dechlorination would have been observed for any of the minerals tested, based on the first-order kinetic rate constants presented in Table 2. Thus, the comparatively slow ferrous mineral correlated reactions observed herein and for natural rock and clayey materials (Schaefer et al., 2013; Schaefer et al., 2018) may be attributable to a mechanism that does not involve RMIs, or may involve RMIs that are far less reactive than those previously observed (Culpepper et al., 2018; Entwistle et al., 2019).

The anoxic dechlorination experiments performed at 0.15 mM TCE concentrations yielded first order rate constants that were approximately 4-times greater than those determined for experiments performed at 3.2 mM TCE. A similar dependence on TCE concentration in clayey soils has been reported (Berns et al., 2019). Thus, while the elevated TCE concentrations used herein and in previous studies (e.g., Schaefer et al., 2018) facilitated the identification and quantification of trace levels of transformation

products, these elevated TCE concentrations likely resulted in an underestimation of the abiotic dechlorination rate constants compared to those rate constants that would have been measured at more dilute TCE concentrations (and that might be more consistent with TCE concentrations at many TCE-impacted field sites). In addition, the dependence of the rate constant on concentration suggests, as previously proposed (Berns et al., 2019), that dechlorination kinetics at elevated TCE concentrations are likely limited by Langmuir-type sorption to reactive mineral sorption sites.

The addition of 1.8 mM dissolved ferrous iron did not impact transformation product formation (i.e., acetylene generation was statistically identical with and without the added ferrous iron, Figure S1 in the Supplemental Information), suggesting that addition of this iron did not result in RMIs that impacted TCE dechlorination. However, as discussed in detail by Entwistle et al. (2019), both the ferrous dosage and geochemical conditions in the batch systems used herein may not have been appropriate for facilitating RMI formation.

The ferrous iron surface-area normalized first-order rate constants (Table 2) as a function of the measured reduction potential are shown in Figure 3. The relationship between reduction potential and the dechlorination rate constant has been estimated as follows (Stewart et al., 2018; Kocur et al., 2019):

$$log(\mathrm{k}_{sa}) = aE + c \qquad \text{Eq. 5}$$

where k_{sa} is the surface-area normalized rate constant (Table 2), a and c are constants, and E is the reduction potential. Kocur et al. (2019) also indicate that a mass-normalized rate constant can be used instead of the surface-area normalized rate constant for more complex sediment matrices (in which it is difficult to get a surface area for the reactive

minerals) in Eq. 5. The surface-area normalized data in Figure 3 are qualitatively consistent with Eq. 5, suggesting the importance of ferrous mineral surfaces for the observed reductive dechlorination reactions when evaluating the data with respect to measured reduction potential. The ferrous iron mass-normalized rate constants do not exhibit a functionality that is consistent with Eq. 5, although the limited number of data points prevents a thorough evaluation of Eq. 5 with respect to reduction of TCE by ferrous minerals. No measurable reductive dechlorination for biotite was observed, which showed a measured reduction potential of +84 mV (vs. SHE); the reduction potential was negative for all other minerals. Thus, the reducing potential of the biotite likely was insufficient to facilitate TCE reduction under the conditions tested. This result highlights a potential useful application of this electrochemical method in identifying ferrous minerals that, despite having apparently sufficient ferrous mineral content as shown in Figure 2, lack the potential to reductively dechlorinate TCE under anoxic conditions.

The results shown in Figures 2 and 3 suggest the importance of considering both the ferrous mineral content and the reduction potential for abiotic TCE reduction under anoxic conditions. While a trend of increasing rate constant with ferrous content is observed in Figure 2, the outlying biotite sample is only explained in the context of its reduction potential. Thus, it is possible that certain ferrous minerals simply do not have sufficient reduction capacity to dechlorinate TCE. It currently is unclear how other geochemical conditions, or the presence of mineral mixtures, may impact dechlorination.

3.2 Oxic Experiments

405 Results showing the generation of hydroxyl radicals are provided in Figure 4. We
406 note that this measure of hydroxyl radical generation is based upon hydroxyl radical
407 reaction with APF, and thus represents only the radicals that are available to react with
408 this compound. The molar hydroxyl radical generation of each mineral was orders of
409 magnitude less than the oxygen present in each vial, so oxygen levels were not limiting
410 and remained essentially constant in the oxic experiments. Because studies using the
411 APF-based approach for hydroxyl radical quantification typically have been performed
412 within approximately 30 hours (e.g., Cohn et al., 2008; Cohn et al., 2009), results shown
413 in Figure 4 are best interpreted by comparing hydroxyl radical generation among the
414 various minerals tested rather than a definitive quantitative value. Comparison of Figures
415 2 and 4 shows that the order of reactivity for the minerals with respect to hydroxyl radical
416 generation differs from that observed for TCE reduction under anoxic conditions. Most
417 notably, illite generates more than twice the hydroxyl radicals than any other mineral,
418 whereas illite's reactivity under anoxic conditions with respect to TCE dechlorination
419 was greater only than biotite (which yielded no measurable TCE dechlorination).
420 Interestingly, biotite exhibited the least amount of reactivity for both the oxic and anoxic
421 conditions.
422 The differences among the mineral reactivities with respect to hydroxyl radical
423 generation are not readily explained by any apparent differences in the mineral properties
424 presented in Table 1. While the high reactivity of the illite appears to correspond to its
425 high specific surface area, the specific surface areas for the other 3 minerals differ by
426 over an order of magnitude, yet differ in only 34% in their hydroxy radical yield over the
427 6-day experiment. Assuming 3 moles of ferrous iron are required to transform TCE to

428 acetylene, and 3 moles of ferrous iron are needed to generate 1 mole of hydroxyl radical
429 (Kong et al., 2015; Schaefer et al., 2018), the fractional ferrous consumption is calculated
430 for each mineral under both oxic and anoxic conditions (Figure 5). Results show that only
431 a relatively small fraction of the ferrous iron was oxidized during both the oxic and
432 anoxic experiments. Furthermore, while the magnitude of the fractional ferrous mineral
433 consumption between the oxic and anoxic experiments was biased to the duration of the
434 experiment (40 days for the anoxic experiments vs. 6 days for the oxic experiments),
435 fractional oxidation of the minerals occurred in the order of illite > biotite > siderite >
436 ankerite (Figure 5), which is the reverse order of their ferrous content (Table 1). The
437 exception is biotite under anoxic conditions which, as previously discussed, likely did not
438 have sufficient reduction potential to reduce TCE.
439 Figure 5 also provides a measure of the molar TCE or oxygen reduced per mole of
440 ferrous iron present in each mineral. Comparison shows that illite is the most reactive
441 mineral (on a mole of TCE or oxygen reacted per mole of ferrous iron) of the four
442 minerals tested. With the exception of TCE reduction via biotite, ankerite shows the least
443 reduction of TCE/oxygen per mole of ferrous iron present. While these relationships are
444 apparent from Figure 5, it is unclear whether these relationships reflect an intrinsic
445 chemical reactivity of the specific ferrous minerals, the available surface area of the
446 ferrous minerals within the bulk mineral structure, the formation of reactive mineral
447 intermediates (Culpepper et al., 2018; Entwistle et al., 2019) within the mineral
448 microstructure, and/or other structural or chemical factors. The fact that the fractional
449 ferrous oxidation in Figure 5 correlates inversely with mineral ferrous content (and also
450 the ratio of the specific surface area to ferrous content) suggests that, for these ferrous

451 rich minerals, the reduction becomes more efficient at lower ferrous contents, potentially
452 due to improved accessibility for TCE and oxygen at reactive mineral surfaces (i.e., less
453 "crowding" of the ferrous iron). Recent investigations by Yuan et al. (2018) show that
454 both surface and structural ferrous iron contributes to hydroxyl radical formation; the
455 similarity in behavior between the oxic and anoxic experiments in Figure 5 suggests that
456 both surface and structural ferrous iron contribute to both the reduction of TCE and
457 oxygen for the minerals examined herein. Additional studies are needed to confirm such
458 mechanisms.
459
460 *3.3 Environmental Implications*
461 Under anoxic conditions, several ferrous mineral types can facilitate TCE reduction,
462 either directly or potentially by the facilitating formation of RMIs. Thus, mineral
463 screening for ferrous content may serve as a useful tool for estimating TCE abiotic
464 dechlorination rate constants in field samples. However, the mineral reduction potential
465 needs to be sufficiently high to induce dechlorination. Thus, a coupled approach
466 involving measurement of both reduction potential and ferrous mineral content offers a
467 likely improved benefit for potentially estimating abiotic reductive dechlorination rate
468 constants in field samples.
469 With respect to oxic conditions, while ferrous minerals appear to play an important
470 role in hydroxyl radical generation, the relationship between ferrous content and mineral
471 properties are currently unclear. Further study is needed to understand this relationship.
472 Overall, the results observed herein and in previous studies (Schaefer et al., 2013;
473 Schaefer et al., 2018) suggest that several ferrous minerals can play a role in the

474 dechlorination of TCE, particularly under anoxic conditions that are typically present
475 within rock or clay matrices. Continued studies with respect to the impacts of
476 geochemical conditions, contaminant mixtures, and potential roles of reactive
477 intermediates on these reactions are needed to further refine understanding of these
478 naturally occurring dechlorination processes.
479
480
481 **Acknowledgments**
482 Support for this research was provided by the Strategic Environmental Research and
483 Development Program (SERDP) under Project ER-2530. Views, opinions, and/or
484 findings contained in this report are those of the authors and should not be construed as
485 an official Department of Defense position or decision unless so designated by other
486 official documentation. The authors appreciate assistance from Veronika Culina in
487 performing the experiments.
488
489
490
491 **References**
492 Arnold, W. A.; Roberts, A. L., 2000. Pathways and kinetics of chlorinated ethylene and
493 chlorinated acetylene reaction with Fe(0) particles. Environ. Sci. Technol. 34,
494 1794−1805.

495 Berns, E.C., Sanford, R.A., Valocchi, A.J., Strathmann, T.J., Schaefer, C.E., Werth, C.J.,
496 2019. Contributions of biotic and abiotic pathways to anaerobic trichloroethene
497 transformation in low permeability source zones. J. Contam. Hydrol. 224, 103480.
498 Butler, E.C., Hayes, K.F., 1999. Kinetics of the transformation of trichloroethylene and
499 tetrachloroethylene by iron sulfide. Environ. Sci. Technol. 33, 2021-2027.
500 Ca piro, N. L.; Löffler, F. E.; Pennell, K. D., 2015. Spatial and temporal dynamics of
501 organohalide-respiring bacteria in a heterogeneous PCE−DNAPL source zone. J.
502 Contam. Hydrol. 182, 78−90
503 Cohn, C.A., Simon, S.R., Schoonen, M.A., 2008. Comparison of fluorescence-based
504 techniques for the quantification of particle-induced hydroxyl radicals. Particle Fibre
505 Toxicol. 5, 2.
506 Cohn, C.A., Pedigo, C.E., Hylton, S.N., Simon, S.R., Schoonen, M.A., 2009. Evaluating
507 the use of 3'-(p-Aminophenyl) fluorescein for determining the formation of highly
508 reactive oxygen species in particle suspensions. Geochem. *Trans.* 10, 8.
509 Culpepper, J.D., Scherer, M.M., Robinson, T.C., Neumann, A., Cwiertny, D., Latta, D.E.,
510 2018. Reduction of PCE and TCE by magnetite revisited. Environ. Sci. Proc. &
511 Impacts 20, 1340-1349.
512 Cussler, E.L., 1994. *Diffusion – mass transfer in fluid systems*, Cambridge University
513 Press.
514 Damgaard, I., Bjerg, P.L., Jacobsen, C.S., Tsitonaki, A., Kerrn-Jespersen, H. and
515 Broholm, M.M., 2013. Performance of full-scale enhanced reductive dechlorination
516 in clay till. Groundwater Monitor. Remed., 33, 48-61.

517 Entwistle, J., Latta, D.E., Scherer, M.M., Neumann, A., 2019. Abiotic Degradation of
518 Chlorinated Solvents by Clay Minerals and Fe (II): Evidence for Reactive Mineral
519 Intermediates. Environ. Sci. Technol. 53, 14308-14318.
520 Fan, D., Bradley, M.J., Hinkle, A.W., Johnson, R.L., Tratnyek, P.G., 2016. Chemical
521 reactivity probes for assessing abiotic natural attenuation by reducing iron minerals.
522 Environ. Sci. Technol. 50, 1868-1876.
523 Ferrey, M.L., Wilkin, R.T., Ford, R.G., Wilson, J.T., 2004. Nonbiological removal of *cis*-
524 dichloroethylene and 1,1-dichloroethylene in aquifer sediment containing magnetite.
525 Environ. Sci. Technol. 38, 1746-1752.
526 Goode, D.J., Imbrigiotta, T.E. and Lacombe, P.J., 2014. High-resolution delineation of
527 chlorinated volatile organic compounds in a dipping, fractured mudstone: Depth-and
528 strata-dependent spatial variability from rock-core sampling. J. Contam. Hydrol., 171,
529 1-11.
530 He, Y.T., Wilson, J.T., Wilkin, R.T., 2010. Impact of iron sulfide transformation on
531 trichloroethylene degradation. *Geochim. Cosmochim. Acta* 74, 2025-2039.
532 He, Y.T., Wilson, J.T., Wilkin, R.T. 2015. Review of Abiotic Degradation of Chlorinated
533 Solvents by Reactive Iron Minerals in Aquifers, Ground Water Monitor. Remed. 35,
534 57-75.
535 Kocur, C.M., Fan, D., Tratnyek, P.G., Johnson, R.L., 2020. Predicting Abiotic Reduction
536 Rates Using Cryogenically Collected Soil Cores and Mediated Reduction Potential
537 Measurements. Environ. Sci. Technol. Letters 7, 20-26.
538 Kong, L., Hu, X. and He, M., 2015. Mechanisms of Sb (III) oxidation by pyrite-induced
539 hydroxyl radicals and hydrogen peroxide. Environ. Sci. Technol. 49, 3499-3505.

Lee, W., Batchelor, B., 2003. Reductive capacity of natural reductants. Environ. Sci. Technol. 37, 535-541.

Liang, X., Philip, R.P., Butler, E.C., 2009. Kinetic and isotope analyses of tetrachloroethylene and trichloroethylene degradation by model Fe(II)-bearing minerals. Chemosphere, 75, 63-69.

Lide, D.R., 1990. *CRC Handbook of Chemistry and Physics*. 71st Edition. CRC Press, Inc.

Liu, X.; Yuan, S.; Tong, M.; Liu, D., 2017. Oxidation of trichloroethylene by the hydroxyl radicals produced from oxygenation of reduced nontronite. Water Res. 113, 72−79.

Morrison, K.D., Misra, R.,Williams, L.B., 2016. Unearthing the antibacterial mechanism of medicinal clay: A geochemical approach to combating antibiotic resistance. *Sci. Reports* 6,19043-19055.

Page, S.E., Kling, G.W., Sander, M., Harrold, K.H., Logan, J.R., McNeill, K., Cory, R.M., 2013. Dark formation of hydroxyl radical in arctic soil and surface waters. Environ. Sci. Technol. 47, 12860-12867.

Pham, H. T.; Kitsuneduka, M.; Hara, J.; Suto, K.; Inoue, C., 2008. Trichloroethylene transformation by natural mineral pyrite: the deciding role of oxygen. Environ. Sci. Technol. 42, 7470−7475.

Rice, E.W., Baird, R.B., Eaton, A.D., Clesceri, L.S., 2012. Standard methods for the examination of water and wastewater. *American Public Health Association: Washington, DC,* USA, 10.

561 Roberts, A. L.; Totten, L. A.; Arnold, W. A.; Burris, D. R.; Campbell, T. J., 1996.
562 Reductive elimination of chlorinated ethylenes by zerovalent metals. Environ. Sci.
563 Technol. 30, 2654−2659.
564 Sander, R. *Compilation of Henry's Law constants for inorganic and organic species of*
565 *potential importance in environmental chemistry*. 1999. Max Plank Institute of
566 Chemistry, Mainz, Germany, www.mpch-mainz.mpg.de/~sander/res/henry.html.
567 Schaefer, C.E., Condee, C.W., Vainberg, S., Steffan, R.J., 2009. Bioaugmentation for
568 chlorinated ethenes using *Dehalococcoides* sp.: comparison between batch and column
569 experiments. Chemosphere 75, 141-148.
570 Schaefer, C.E., Towne, R.M., Lippincott, D.R., Lazouskaya, V., Fischer, T.B., Bishop,
571 M.E., Dong, H., 2013. Coupled diffusion and abiotic reaction of trichloroethene in
572 minimally disturbed rock matrices. Environ. Sci. Technol., 47, 4291-4298.
573 Schaefer, C.E., Towne, R.M., Lippincott, D.R., Lacombe, P., Bishop, M.E., Dong, H.,
574 2015. Abiotic Dechlorination in Rock Matrices Impacted by Long-Term Exposure to
575 TCE. Chemosphere 119, 744-749.
576 Schaefer, C.E., 2016. Naturally occurring dechlorination reactions in rock matrices:
577 impacts on TCE fate and flux. Environ. Technol. Innovation 6, 115-122.
578 Schaefer, C.E., Ho, P., Gurr, C., Berns, E., Werth, C., 2017. Abiotic dechlorination of
579 chlorinated ethenes in natural clayey soils: Impacts of mineralogy and temperature. J.
580 Contam. Hydrol., 206, 10-17.
581 Schaefer, C.E., Ho, P., Berns, E., Werth, C., 2018. Mechanisms for abiotic
582 Dechlorination of Trichloroethene by ferrous minerals under Oxic and anoxic
583 conditions in natural sediments. Environ. Sci. Technol. 52, 13747-13755.

584 Schaefer, C.E., Lippincott, D.R., Klammler, H., Hatfield, K., 2018b. Evidence of rock
585 matrix back-diffusion and abiotic dechlorination using a field testing approach. J.
586 Contam. Hydrol. 209, 3-41.
587 J Środoń J., 1978. Illite group clay minerals. In: Middleton G.V., Church M.J., Coniglio
588 M., Hardie L.A., Longstaffe F.J. (eds) Encyclopedia of Sediments and Sedimentary
589 Rocks. Encyclopedia of Earth Sciences Series. Springer, Dordrecht.
590 https://doi.org/10.1007/978-1-4020-3609-5_115
591 Stewart, S.M., Hofstetter, T.B., Joshi, P., Gorski, C.A., 2018. Linking thermodynamics to
592 pollutant reduction kinetics by Fe2+ bound to iron oxides. Environ. Sci. Technol. 52,
593 5600-5609.
594 Tong, M., Yuan, S., Ma, S., Jin, M., Liu, D., Cheng, D., Liu, X., Gan, Y.,Wang, Y., 2016.
595 Production of abundant hydroxyl radicals from oxygenation of subsurface sediments.
596 Environ. Sci. Technol, 50, 214-221.
597 West, M.R. and Kueper, B.H., 2010. Plume detachment and recession times in fractured
598 rock. Groundwater 48, 416-426.
599 Werth, C.J., Cunningham, J.A., Roberts, P.V. and Reinhard, M., 1997. Effects of grain-
600 scale mass transfer on the transport of volatile organics through sediments: 2. Column
601 results. Water Resour. Res. 33, 2727-2740.
602 Yu, R., Andrachek, R.G., Lehmicke, L.G., Freedman, D.L., 2018. Remediation of
603 chlorinated ethenes in fractured sandstone by natural and enhanced biotic and abiotic
604 processes: A crushed rock microcosm study. Sci. Total Environ. 626, 497-506.

605 Yuan, S., Liu, X., Liao, W., Zhang, P., Wang, X., Tong, M., 2018. Mechanisms of
606 electron transfer from structrual Fe (II) in reduced nontronite to oxygen for production
607 of hydroxyl radicals. Geochim. Cosmochim. Acta, 223, 422-436.
608 Yuan, X., Nico, P.S., Huang, X., Liu, T., Ulrich, C., Williams, K.H., Davis, J.A., 2017.
609 Production of hydrogen peroxide in groundwater at Rifle, Colorado. Environ. Sci.
610 Technol. 51, 7881-7891.
611 Zhu, A., Guo, Y., Liu, G., Song, M., Liang, Y., Cai, Y., Yin, Y., 2019. Hydroxyl radical
612 formation upon dark oxidation of reduced iron minerals: Effects of iron species and
613 environmental factors. Chinese Chem. Letters 30, 2241-2244.
614

615 # Tables

Table 1. Mineral properties for the four minerals used in this study. Mineral formulas from Lide (1990) and Środoń (1978).

Property	Ankerite $[Ca(Fe, Mg, Mn)(CO_3)_2]$	Siderite $[FeCO_3]$	Biotite $[K(Mg, Fe)_3AlSi_3O_{10}(OH, F)_2]$	Illite $[K_{1-1.5}Al_4(Mg, Fe)Si_{7-6.5}Al_{1-1.5}O_{20}(OH)_4]$
% Mineral Content (XRD analysis)[1]	Ankerite (96.4); Calcite (3.6)	Siderite (94.7); Quartz (3.7); illite+mica (1.7)	Biotite (100)	Illite+mica (51.6); Quartz (18.3); Calcite (13.6); K-Feldspar (5.4); Chlorite (4.2); Pagioclase (4.0); Gypsum (2.2)
Avg. Particle Size (µm)	64	32	18	~1[2]
Specific Surface Area[3] (m^2/g)	0.64	9.7	2.0	64
Ferrous mineral content[4] (g/kg)	170 [180]	36 [410]	2.0 [47]	0.46 [3.6]
Reduction Potential (mV) vs. SHE	-102	-9.0	+84	-104
pH[5]	7.6	6.4	8.7	7.8

[1] XRD analyses performed by the Premier Oilfield Group (Houston, TX). Only minerals with >1% abundance are shown.

[2] 55% of the particle mass was <1 µm, as determined via sieve analysis.

[3] Nitrogen-BET (Brunauer-Emmett-Teller) adsorption analysis performed by Particle Technology Labs (Downers Grove, IL)

[4] The first value is based on Standard Method 3500-Fe B.4.c. (Rice et al., 2012), while the bracketed value uses a more concentrated (12.5%) HCl solution and heating to 95 C. Analyses were performed by McCampbell Analytical, Inc.

[5] pH sample collected from the supernatant aqueous phase in the vials at the end of the experiment.

Table 2. Regressed first order rate constants for reductive TCE dechlorination under anoxic condition derived from the acetylene and ethene gas generation data. The ± values indicate the 95% confidence intervals. NA=not applicable. No dechlorination was measured for biotite.

Mineral	Initial TCE Concentration (mM)	Rate Constant[1] ($L\ g^{-1}\ d^{-1}$)	Rate Constant[2] ($L\ m^{-2}\ d^{-1}$)	R^2
Ankerite	3.2	$1.3 \pm 0.22 \times 10^{-7}$	$1.2 \pm 0.20 \times 10^{-6}$	0.99
Siderite[3]	3.2	$1.2 \pm 0.32 \times 10^{-7}$	$3.5 \pm 0.94 \times 10^{-7}$	0.98
	0.15	$4.8 \pm 0.45 \times 10^{-7}$	$1.4 \pm 0.13 \times 10^{-6}$	0.99
Biotite	3.2	0	0	NA
Illite	3.2	$3.1 \pm 1.3 \times 10^{-8}$	$1.1 \pm 0.46 \times 10^{-6}$	0.92
	0.15	$1.5 \pm 0.64 \times 10^{-7}$	$5.0 \pm 2.1 \times 10^{-6}$	0.89

[1] Mass normalized rate constants are calculated by dividing k_{an} (Eq. 2) by the mineral mass (g) per L water in the batch experiments, thereby normalizing rate constants for comparison among batch studies using different solid dosages, as shown in Figure 2.

[2] Ferrous iron surface area normalized rate constants are calculated by diving k_{an} (Eq. 2) by the ferrous mineral specific surface area per L in the batch experiments. The ferrous mineral surface area is estimated by assuming the fraction of ferrous surface area to the total measured surface area (Table 1) is equal to the mass fraction of ferrous iron in the mineral (based on 2.5% HCl extractions).

[3] The t=1 day data were not used in the regressions for siderite.

FIGURES

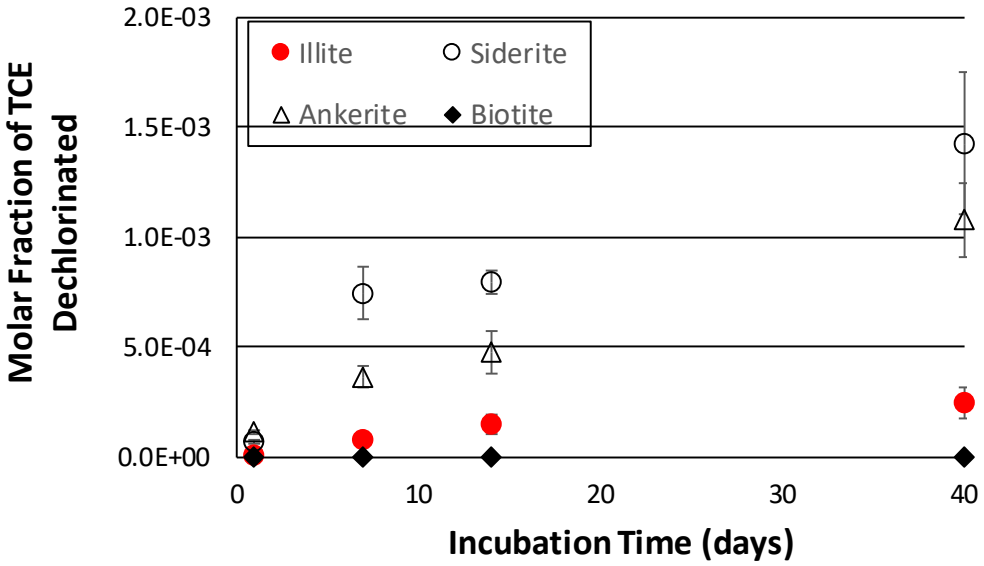

Figure 1. Reduced gas TCE dechlorination products as a molar fraction of the initial TCE added to the vials (moles dechlorination product / moles initial TCE). TCE dechlorination was based on acetylene and ethene generation. Average values are shown. Error bars represent the 95% confidence interval.

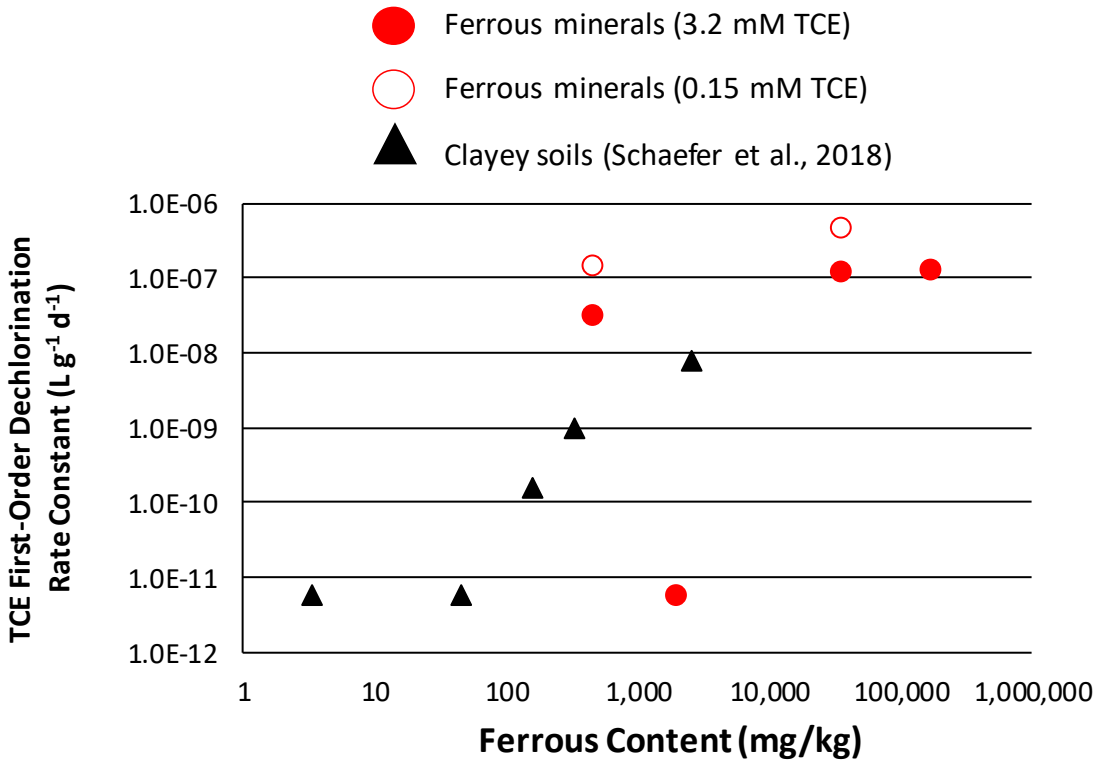

653

654 **Figure 2.** First-order rate constants describing TCE reductive dechlorination under
655 anoxic conditions (derived from the triplicate data in Figure 1 and the regressions shown
656 in Table 2). Ferrous contents were determined using Standard Method 3500-Fe B.4.c.
657 (2.5% HCl extractions), as shown in Table 1. Data attained herein (Table 2) at two
658 different initial TCE concentrations and from Schaefer et al. (2018) are shown. Values
659 plotted less than 10^{-11} L g^{-1} d^{-1} represent experiments where no measurable dechlorination
660 was observed.
661
662
663
664
665

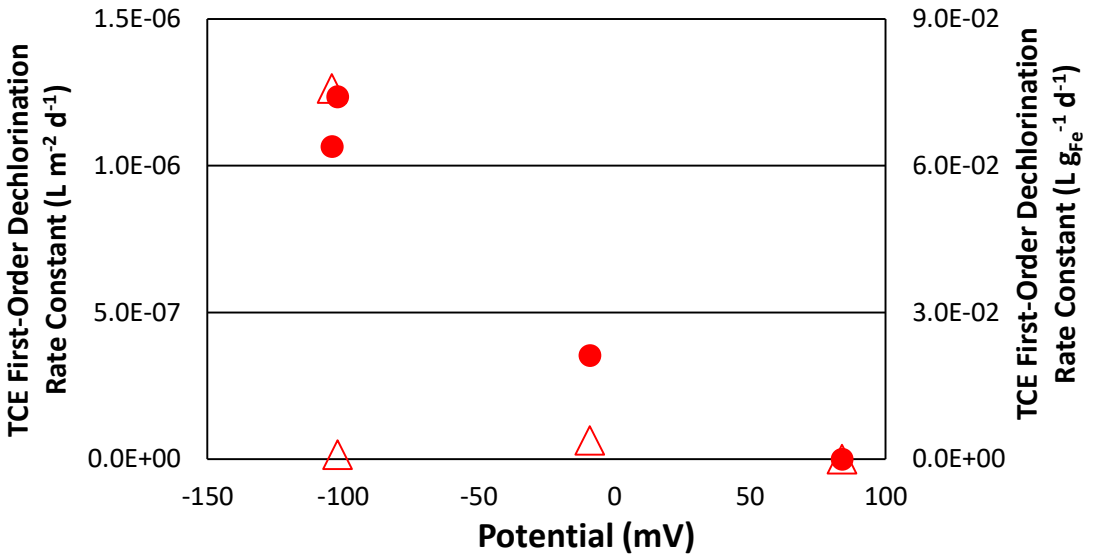

666

667 **Figure 3.** TCE reductive dechlorination first-order rate constants (Table 2) under anoxic
668 conditions as a function of the measured reduction potential (vs. SHE). Surface area-
669 normalized rate constants listed in Table 2 (filled circles) are plotted on the primary
670 vertical axis, and ferrous iron mass-normalized rate constants (mass normalized rate
671 constants in Table 1 divided by the ferrous iron content determined using 2.5% HCl) are
672 plotted on the secondary vertical axis as open triangles. Reduction potentials are averages
673 of duplicate (at least) measurements that varied by less than 10%.

674

675
676
677
678

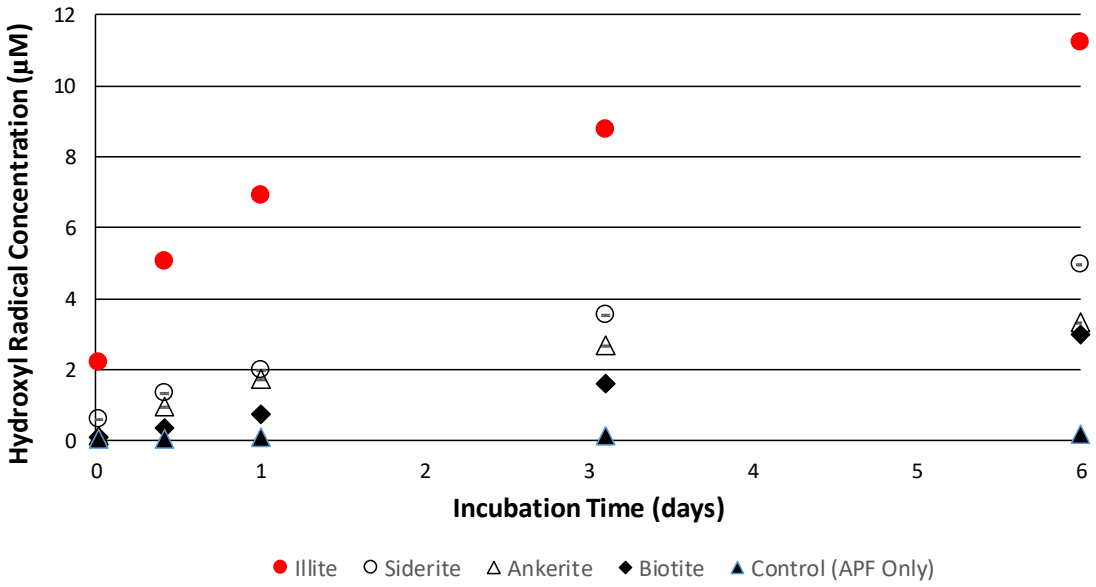

Figure 4. Hydroxyl radical generation in the oxic experiments. Average of duplicate experiments are shown. Error bars, which are typically smaller than the data markers, represent 95% confidence intervals.

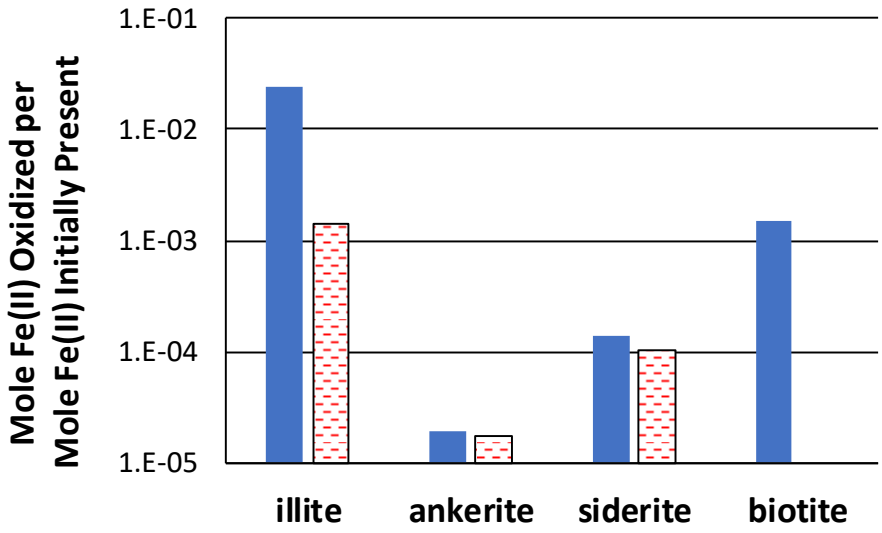

689

690 **Figure 5.** Fraction of ferrous iron oxidized by either TCE (solid blue bars) or oxygen
691 (dashed pattern bars), based on ferrous mineral content via Standard Method 3500-Fe
692 B.4.c. (Rice et al., 2012) shown in Table 1, and the amount of either acetylene (anoxic) or
693 hydroxyl radical (oxic) generated. Results are shown for each mineral tested.

694

695

Graphical Abstract